Research Article

Open Access

A. Richter*, L. Müller, E. Marderwald, L. Mendoza, E. Kruse, S. Perdomo, M. Scheinert, and R. Perdomo

Towards a tidal loading model for the Argentine-German Geodetic Observatory (La Plata)

Abstract: We present a regionalized model of ocean tidal loading effects for the Argentine-German Geodetic Observatory in La Plata. It provides the amplitudes and phases of gravity variations and vertical deformation for nine tidal constituents to be applied as corrections to the observatory's future geodetic observation data. This model combines a global ocean tide model with a model of the tides in the Río de la Plata estuary. A comparison with conventional predictions based only on the global ocean tide model reveals the importance of the incorporation of the regional tide model. Tidal loading at the observatory is dominated by the tides in the Atlantic Ocean. An additional contribution of local tidal loading in channels and groundwater is examined. The magnitude of the tidal loading is also reviewed in the context of the effects of solid earth tides, atmospheric loading and non-tidal loads.

Keywords: fundamental station, geodesy, gravimetry, ocean tidal loading, Río de la Plata

*Corresponding Author: A. Richter:** Laboratorio MAGGIA, Facultad de Ciencias Astronómicas y Geofísicas, Universidad Nacional de La Plata, Argentina
and Consejo Nacional de Investigaciones Científicas y Técnicas, Argentina, E-mail: richter.a@daad-alumni.de
L. Müller, M. Scheinert: Institut für Planetare Geodäsie, Technische Universität Dresden, Germany
E. Marderwald, L. Mendoza: Laboratorio MAGGIA, Facultad de Ciencias Astronómicas y Geofísicas, Universidad Nacional de La Plata, Argentina
and Consejo Nacional de Investigaciones Científicas y Técnicas, Argentina
E. Kruse: Consejo Nacional de Investigaciones Científicas y Técnicas, Argentina
and Facultad de Ciencias Naturales y Museo, Universidad Nacional de La Plata, Argentina
S. Perdomo: Consejo Nacional de Investigaciones Científicas y Técnicas, Argentina
and Facultad de Ciencias Naturales y Museo, Universidad Nacional de La Plata, Argentina

1 Introduction

The Argentine-German Geodetic Observatory (AGGO) is currently being set up some 20 km west of La Plata city [1]. When operative, it will be a geodetic fundamental station combining the observation techniques Very Long Baseline Interferometry (VLBI), Satellite Laser Ranging (SLR), Global Navigation Satellite Systems (GNSS, at present the Global Positioning System and GLONASS) and continuous gravimetry with a superconducting gravity meter. The colocation of these complementary techniques contributes to the realization of global geodetic reference systems. In addition, a continuous stream of observation data from AGGO's instruments will allow in future the investigation of numerous processes vital in the earth system. One prerequisite to achieve the necessary accuracy is the reduction of the observations for the effects of earth tides and ocean-tidal loading. The movement of water mass caused by the ocean tides generates periodic variations in local gravity, clearly visible in gravimetric records, and vertical (and – much smaller – horizontal) displacements of the earth surface, which affect the geometric observation techniques VLBI, SLR and GNSS. These periodic variations can mask the contribution of many other phenomena to the observation data and should be removed prior to an interpretation of the observations with regard to non-tidal processes [2].

The geographical setting of AGGO is characterized by a low and very flat topography, the proximity of the Río de la Plata estuary and a substrate consisting of loose sediments (Fig. 1). Along the shore of the Río de la Plata dikes and channels reach inland. The estuary is shallow and subject to peculiar hydrodynamics [3, 4]. It participates in the

and Facultad de Ciencias Astronómicas y Geofísicas, Universidad Nacional de La Plata, Argentina
R. Perdomo: Facultad de Ciencias Astronómicas y Geofísicas, Universidad Nacional de La Plata, Argentina

ocean tides with substantial modulation of the tidal signal compared to the nearby Atlantic Ocean [5]. Satellite altimetry is the principal data source for recent global ocean tide models [6]; but its applicability over the narrow Río de la Plata is very limited because standard procedures do not provide reliable sea-surface heights in coastal waters [7]. [8] derived a regional tide model for the estuary from tide gauge records at 34 sites. Figure 2 illustrates the local conditions for tidal loading at AGGO through amplitude spectra of the water-level variations at the tide gauge at La Plata port (top) and the predicted atmospheric loading effect on gravity at AGGO (bottom) according to the ATMACS model (http://atmacs.bkg.bund.de/data/results/icongl/lp2016_icon384_200km.grav) [9].

Operational tools are available to compute ocean tidal loading corrections, for example the Ocean Tide Loading Provider [10] or the SUMMARYA model [11]. However, these tools employ only a range of global ocean tide models and thus, does not allow to adequately account for the particular situation in the vicinity of the Río de la Plata. Here, we derive corrections for the location of AGGO based on a regionalized modelling of ocean tidal loading effects. This model incorporates the estuary tide model from [8]. We explore the loss of accuracy in the corrections when using global models only, as well as the potential impact of additional local and regional effects.

2 Methods

2.1 Modelling ocean tidal loading effects

Ocean tidal loading is a particular case of surface loading. The mass of water redistributed in the ocean and seas by the ocean tides generates a load potential and acts as a surface force on the solid earth. This results in a number of effects, such as variations in local gravity, tilt and deflection of the vertical, vertical and horizontal deformation of the surface of the solid earth, among others, with the same persistent periods as the ocean tidal forcing. Tidal periods, dominated by diurnal and semi-diurnal constituents, are short compared to the visco-elastic relaxation time of the solid earth. For this reason, the modelling of ocean tidal loading effects usually accounts for the purely elastic response only. These effects are calculated as a convolution integral of an elastic earth model with a load model. The earth model quantifies the response of the solid earth to a surface force while the load model describes the mass displacement in space and time. We apply the Green's functions tabulated in [12] for the Gutenberg-Bullen SNREI

earth model with respect to a CE frame (fixed center of mass of the solid earth [13]). As load models we use grids of global, regional and local extent (Fig. 1) that contain the complex amplitudes of water-level variations for nine tidal constituents: Q1, O1, P1, K1, N2, M2, S2, K2 and M4. The convolution is realized by an own implementation. The correctness of our calculus was proven by a global comparison with the Ocean Tide Loading Provider and the NLOADF algorithm of the SPOTL package [14] yielding maximum differences of 3% and 1° for amplitudes and phases, respectively. Finally, the complex amplitudes resulting from the convolution were converted to amplitudes A and phases G. In the following, we focus our ocean tidal loading computations on the location of AGGO and on two observable effects: local gravity change (as observed by gravity meters) and vertical crustal deformation (as observed by the geometric techniques GNSS, SLR and VLBI).

2.2 Load model components

The tidal load of the Río de la Plata estuary and the far-field contribution of the global ocean are considered as separate load model components. The convolution is done individually for both components. The final ocean tidal loading effects are obtained by summation of the contributions of both components. The load model components differ not only in their geographical domains, but also in their grid resolution and the data source of the underlying tide models. The regional SEAT model by [8] is used to represent the tides in the Río de la Plata estuary. This model is based on tide gauge observations and has a grid spacing of approximately 500 m. The SW shoreline of the estuary was digitized from georeferenced satellite imagery. We checked the land-water mask of the SEAT model against this high-resolution shoreline polygon and found an excellent agreement. From this model only one long-period tidal constituent, Sa, is available. However, the water-level variations in the estuary with annual period are dominated by the seasonal hydrological cycle, primarily due to run-off variations of the Paraná River. This, in turn, is subject to significant interannual fluctuations. Hence, we do not include any long-period constituent in the following tidal loading modelling.

The EOT11a global ocean tide model [15] is used to account for the tidal load of the global ocean. This empirical ocean tide model is based on multi-mission satellite altimetry and is given on a global grid of 1/8 degree spacing. The grid cells of the global model that fall within the bounds of the regional SEAT model are masked out in order to ensure a consistent nesting of both model compo-
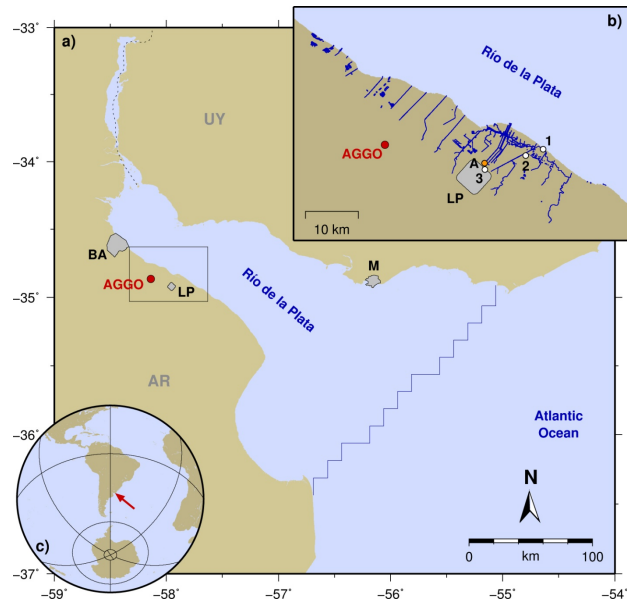
Figure 1: Map of the area under investigation. a) Map of the Río de la Plata estuary. Red dot: location of AGGO (34º51.98' S, 58º08.39' W, 20 m a.m.s.l.); jagged blue line: boundary between the regional (SEAT) and global (EOT11a) load model components in the computation of tidal loading effects; black box: area shown in inset b); grey patches: cities of Buenos Aires (BA), La Plata (LP) and Montevideo (M). b) Detailed map of the surroundings of AGGO and La Plata. Red dot: location of AGGO; dark blue polygons: channels and water bodies considered as local load model component; white dots: location of three groundwater gauges; orange dot: location of water level observations; grey square: centre of La Plata city (LP). c) Inset showing the location of the Río de la Plata estuary at the Atlantic coast of South America (red arrow).

nents. In order to investigate the dependence of the local ocean tidal loading effects at AGGO on the choice of the tide model representing the global ocean, the computation was repeated replacing the EOT11a model by two alternative global ocean tide models: EOT08a (a precursor of the EOT11a model; [16]) and TPXO.7.2 [17].

In addition, we attempt to quantify the potential impact of a propagation of the tidal water-level signal through the channels and dikes from the Río de la Plata inland. Due to the minuscule slope of the water courses and the closeness to which some of them approach the AGGO site, such a local contribution may not be excluded a-priori. For this purpose, we digitized also the contours of 167 water bodies potentially participating in the tides along the SW shore of the estuary between 57º36' and 58º18' W. For each of these water bodies an individual high-resolution grid is derived. All water-covered cells of this grid contain the complex amplitudes of the nine considered tidal constituents as predicted by the regional SEAT model for the location of the mouth of this water

body. In this way, we assume an undamped, instantaneous participation of the entire water body in the tidal signal in the estuary. The disregard of damping of the tidal amplitudes in the channels represents a maximum scenario and thus provides an upper bound estimate for the effects of the local tidal loading.
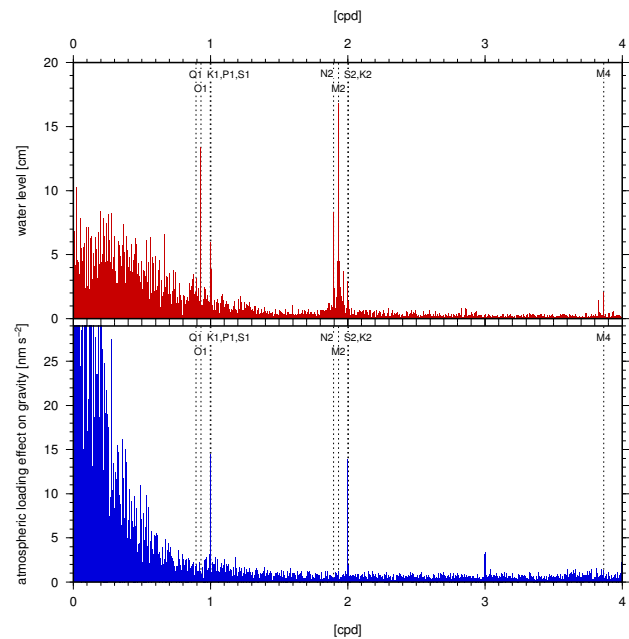

Figure 2: Top: Amplitude spectra of water-level variations recorded at La Plata port tide gauge (284 days, 20 min interval). Bottom: Amplitude spectra of the atmospheric loading effect on gravity at AGGO according to the ATMACS model (354 days, 3 h intervall, includes the effect of atmospheric loading deformation). The frequencies corresponding to the tidal constituents considered in this work are indicated by dashed lines.

Figure 3 demonstrates the effect of the slope on the tidal signal in such a channel. At an upstream location the tidal range is truncated because the minimum water level does not develop completely at low tide. Thus, the harmonic analysis of a tidal record at this location yields a reduced amplitude. At the same time, higher harmonics (i.e. M4 and M6 in the case of M2) increase in amplitude. The magnitude of this effect depends on the original (i.e. without truncation) amplitude and is thus different for each tidal constituent.

In order to put the magnitude of the tidal loading in a context with other relevant contributions, some additional effects were modelled for the AGGO site: The effects of the solid earth tides on local gravity and vertical deformation were modelled using the ETGTAB tool of the ETERNA 3.4 package [18]. The atmospheric loading effect on the vertical deformation on the tidal S1 and S2 frequencies were
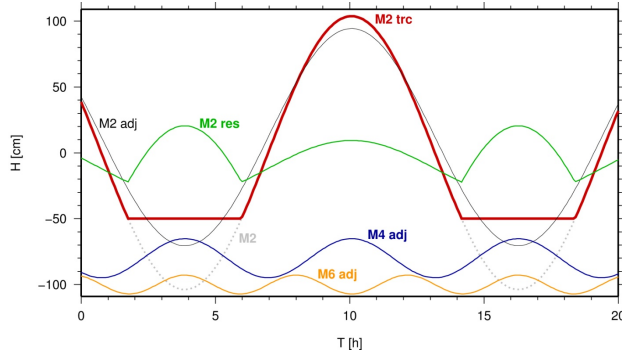
Figure 3: Simulation of the effect of slope on the M2 tidal signal at an upstream (elevated) location of a channel connected to the estuary over 20 h. Dashed grey line: undisturbed tidal signal of the M2 constituent in the estuary (M2); red line: truncated tidal signal observed at the elevated position (M2 trc); thin black line: M2 signal derived by harmonic tidal adjustment from the truncated signal M2 trc (M2 adj); green line: residuals of the truncated M2 signal M2 trc after subtraction of the extracted M2 signal M2 adj (M2 res = M2 trc - M2 adj); blue line: M4 signal derived by harmonic tidal adjustment solely from the truncated signal M2 trc (M4 adj); yellow line: M6 signal derived by harmonic tidal adjustment solely from the truncated signal M2 trc (M6 adj).

derived from the model [19] (without Center of Mass Correction). Atmospheric loading effects on gravity were examined using the ATMACS model time series. Finally, a global convolution of the AOD1B GRACE de-aliasing product (http://www.gfz-potsdam.de/en/aod1b) was used to quantify the vertical deformation due to non-tidal atmospheric and ocean loading [20].

2.3 Intercomparison of load tide models

For a quantitative comparison we also retrieved predictions from the Ocean Tide Loading Provider (without Center of Mass Correction) employing a series of recent global ocean tide models, in particular: EOT11a [15], EOT08a [16], OSU12 [21], TPXO.7.2 [17], FES2012 [22], FES2004 [23] and DTU10 [24]. All these models comprise the eight diurnal and semi-diurnal constituents Q1, O1, P1, K1, N2, M2, S2, K2 in common with our regionalized model. For each of the models M and constituents w the RMS (root mean square) of the differences with respect to our regionalized model (index 0) was computed as [25]

$$RMS_w^M = \sqrt{\left[\left(Re_w^M - Re_w^0 \right)^2 + \left(Im_w^M - Im_w^0 \right)^2 \right] \Big/ 2},$$

with $Re = A \cos G$; $Im = A \sin G$.

These RMS differences were summed up to the RSS (root sum square) as a global measure of misfit of each

model M according to

$$RSS^M = \sum_w \left(RMS_w^{M^2} \right).$$

Furthermore, the different load tide models were expanded in the time domain using the tidal prediction tool MARIE of the TASK-2000 software package [26] for the period 2016-2036 (i.e., completing one lunar nodal cycle) with a resolution of 1 min. In the differential time series of these models minus our load tide prediction, the maximum and minimum deviations were extracted as worst-case difference of the effects. From these differential time series, daily mean differences were derived and their maximum and minimum values determined as a measure of the impact of the choice of a particular set of tidal loading parameters on daily position solutions (e.g. from GNSS).

3 Results

The amplitudes A_g and phases G_g of the tidal loading effect on the local gravity at the AGGO site for the nine considered tidal constituents are shown in Table 1. This table includes also the amplitudes of the solid earth tide effect as predicted by the ETERNA 3.4 software [18]. The phases are given in both global phase lag G relative to the 0° meridian and local phase lead L. In addition, the contributions of the global and regional load model components are specified individually.

In a similar way, Table 2 shows the amplitudes A_u and global phase lags G_u for the nine tidal constituents of the tidal loading effect on the vertical deformation at the AGGO site. Again, the individual contributions of the two load model components are given. This tidal loading deformation refers to the CE frame [13]. The relation between the contributions of both load model components and solid earth tide to gravity and vertical deformation is depicted in Fig. 4 for the M2 constituent.

4 Discussion

Our results suggest that the contribution of the Río de la Plata estuary to the local tidal loading effects at the AGGO site is small compared to that of the global ocean. The amplitudes of the estuary contribution reach on average only 2.5% of that of the ocean. The phase of the estuary contribution is shifted by roughly 180° against the ocean contribution and thus reduces the total effect. We explain the small impact of the estuary, despite its closeness to

Table 1: Ocean tidal loading effect on local gravity variations at AGGO derived from tide model SEAT combined with EOT11a. A_g: amplitude of the tidal loading effect on gravity; G_g: global phase lag (w.r.t. 0° meridian) of tidal loading; A_{set}: amplitude of solid earth tide gravity variation; L_g: local phase lead (as used in tidal gravimetry) of tidal loading; A_{glo}, G_{glo}: amplitude and global phase lag of the contribution of the open ocean to tidal loading gravity signal at AGGO; A_{reg}, G_{reg}: amplitude and global phase lag of the contribution of the tides in the Río de la Plata estuary to tidal loading gravity signal.

Tidal wave	A_g [nm s^{-2}]	G_g [°]	A_{set} [nm s^{-2}]	L_g [°]	A_{glo} [nm s^{-2}]	G_{glo} [°]	A_{reg} [nm s^{-2}]	G_{reg} [°]
Q1	2.63	48.29	55.75	9.65	2.61	46.17	0.10	126.02
O1	10.20	61.01	291.20	-3.08	10.30	59.37	0.31	168.82
P1	2.70	64.68	135.49	-6.75	2.71	65.10	0.02	303.48
K1	7.67	74.31	409.54	-16.38	7.69	74.88	0.08	329.42
N2	3.55	271.74	96.77	24.13	3.67	269.45	0.18	39.37
M2	10.77	270.87	505.45	25.00	11.22	270.39	0.46	79.09
S2	2.04	258.55	235.16	37.31	2.05	260.66	0.08	164.49
K2	0.30	214.42	63.92	81.44	0.28	217.78	0.03	178.55
M4	0.23	161.75	0.12	69.99	0.26	158.93	0.03	318.38

Table 2: Ocean tidal loading effect on vertical deformation w.r.t. a CE frame at AGGO derived from tide model SEAT combined with EOT11a; A_u, G_u: amplitude and global phase lag of the tidal loading effect on the vertical position; A_{glo}, G_{glo}: amplitude and global phase lag of the contribution of the open ocean to tidal loading deformation signal at AGGO; A_{reg}, G_{reg}: amplitude and global phase lag of the contribution of the tides in the Río de la Plata estuary to tidal loading deformation signal.

Tidal wave	A_u [mm]	G_u [°]	A_{glo} [mm]	G_{glo} [°]	A_{reg} [mm]	G_{reg} [°]
Q1	1.07	221.21	1.07	219.28	0.04	305.35
O1	4.21	232.93	4.26	231.54	0.11	348.19
P1	1.17	236.94	1.17	237.33	0.01	122.78
K1	3.28	241.77	3.28	242.28	0.03	148.30
N2	1.47	81.34	1.52	79.59	0.07	219.17
M2	4.99	77.24	5.16	77.29	0.17	258.77
S2	1.38	67.48	1.38	68.64	0.03	344.33
K2	0.32	47.56	0.32	48.97	0.01	358.33
M4	0.08	338.38	0.09	335.91	0.01	138.45

Figure 4: Phasor plots of the modelled contributions to tidal gravity variation (top) and vertical deformation (bottom) for the M2 constituent at AGGO. Thin black vectors: solid earth tide contribution; blue vector: tidal loading contribution from the open ocean (EOT11a); red vector: tidal loading contribution from the tides in the Río de la Plata estuary; black boxes: outline of the section shown in the following panel. A_g and A_u denote the amplitudes of gravity variation and vertical deformation, respectively, G: global phase lag w.r.t. the 0° meridian. a) Total M2 gravity variation. b) Zoom into a), focussing on the global ocean contribution. Grey vector: tidal loading signal predicted by the Ocean Tide Loading Provider based on the EOT11a tide model only. c) Zoom into b), focussing on the estuary contribution. d-f) Same as a-c for the M2 vertical deformation.

the site of interest, by a) the relatively small tidal amplitudes in the estuary compared to large parts of the Argentine coast; b) the relatively small width of the estuary near the AGGO site, which represents only a small fraction of the surrounding area, implying a rather small mass in the immediate vicinity of AGGO contributing to the load; and c) the phase shift of roughly 360° of the tidal consituents along the estuary from its mouth to the head resulting in a compensation of the contributions of different parts of the estuary.

Figure 4 shows that the tidal loading effects are between one and two orders of magnitude smaller than the
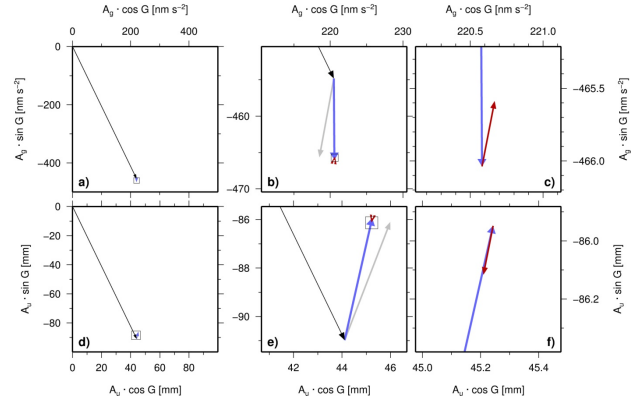
effects of the solid earth tide. The tidal loading increases the gravity signal of the solid earth tide but reduces the earth tide deformation.

Tables 3 and 4 summarize the differences between our tidal loading model and a series of alternative predictions. They reveal mean RSS differences of 25.0 ±0.3 nm s^{-2} and 0.57 ±0.19 mm in gravity and vertical deformation, respectively, for the predictions of the Ocean Tide Loading

Provider using seven different global ocean tide models. In contrast, these RSS amount to only 0.7 nm s^{-2} and 0.14 mm for the two alternative predictions that include the SEAT model in addition to two different global tide models. This indicates the importance of the incorporation of the regional load model component in the computation of precise tidal loading effects for the AGGO site.

The bias resulting from the neglect of the tidal regime in the estuary is more pronounced for the gravity effect than for the vertical deformation. The consistency found among the different global ocean tide models considered here suggests, on the other hand, that the specific choice of the model used to represent the ocean's far-field contribution is of minor importance.

The regional tide model SEAT, and thus the derived tidal loading signals, are not error-free. We used unpublished pressure tide gauge records of six months duration at six offshore locations in the estuary to assess the uncertainty of the tide model and its impact on the tidal loading parameters. These locations cluster within 5 km from the Argentine bank between Buenos Aires city and the AGGO site and were not included in the compilation of the SEAT model. The differences between the observed tides and the predictions of SEAT, averaged over the six sites, yield a RSS of 5.7 cm for the nine constituents considered in this work. We averaged the deviations of SEAT from the observed tides for each constituent individually over the six tide gauge locations and applied them as constant "corrections" all over the estuary (SEAT model domain). This yields changes in the ocean tidal loading parameters that sum up to RSS of 0.48 nm s^{-2} and 0.18 mm for the gravity change and vertical deformation, respectively. This difference is comparable to that implied by replacing the far-field contribution of a global ocean tide model when combined with the regional SEAT model (cf. columns 2 and 3 in Tables 3 and 4) and is much smaller (two orders of magnitude for gravity) than predictions relying on global models only. The distribution of our tide gauge sites does not provide a realistic picture of the performance of SEAT all over the estuary. Nevertheless, it samples the part of the estuary most relevant for tidal loading at AGGO. At the same time, this part close to the head of the estuary is that of the largest spatial gradients and variability and thus the most challenging for tide modelling. The broad waters closer to the mouth are expected to be less affected by interpolation and modelling errors [8]. In addition, the tidal parameters derived from the tide gauge records are subject to uncertainties, too, but this is not accounted for in our assessment. We therefore consider our uncertainty estimate as conservative.

Predictions of the Ocean Tide Loading Provider using the FES2004 global ocean tide model are in wide use in the field of GNSS data processing [2]. In most of the cases, daily position solutions are derived. We estimate that the difference between this prediction and our tidal loading model results in differences in daily mean vertical positions that vary over 20 years within ±0.08 mm.

Table 3 also shows that the local load model contribution of the channels and dikes are negligible. Our maximum scenario estimate, assuming an undamped participation of these water bodies in the tidal signal in the estuary, yields contributions to the gravity and vertical deformation that remain within ±0.05 nm s^{-2} and ±0.02 mm, respectively. These numbers are, in fact, an overestimation, since water level observations at site A (Fig. 1b) revealed no tidal influence. A significant additional contribution from a propagation of the tidal signal through the groundwater from the estuary inland is not expected. We examined water level records from three groundwater gauges at different distances from the shore of the estuary. The sites are shown in Fig. 1 b (1-3). In the groundwater variations at site 1, within 50 m to the shore, tides are observed. However, the groundwater signal is substantially damped even this close to the estuary with an M2 amplitude of 1.6 cm compared to 24.5 cm in open water. At the more distant groundwater gauges at sites 2 und 3, the tidal amplitudes do not exceed the overall noise level (i.e. 2 mm).

The so-called tidal atmospheric loading adds to the ocean tidal loading effects presented in Tables 1 and 2. Atmospheric loading originates, in fact, from radiative rather than gravitative forcing and is thus primarily effective on the harmonics of the solar day S1 and S2. According to the ATMACS model [9] this atmospheric loading effect on gravity (incuding the effect of atmospheric loading deformation on gravimetric observations) reaches amplitudes of 14.5 nm s^{-2} and 13.9 nm s^{-2} for the S1 and S2 constituents, respectively (Fig. 2, bottom). These amplitudes exceed those of the ocean tidal effect on gravity (cf. Table 1). Apart from the solar day harmonics, the amplitudes of the predicted atmospheric loading remain below an almost constant level of 1 nm s^{-2}. In particular, except for S2, a significant alteration of the tidal loading parameters for the constituents presented in Table 1 from persistant atmospheric loading is not expected. Significant non-tidal atmospheric loading occurs with periods of a few days or more (Fig. 2, bottom).

Tidal atmospheric loading produces also vertical deformations with amplitudes of 0.84 mm and 0.72 mm for S1 and S2, respectively, according to the model of [19]. This is roughly an order of magnitude smaller than the ampli-

Table 3: Comparison of alternative predictions of tidal loading effects on gravity with respect to the model used in Table 1. For each model, the root sum square (RSS) of the RMS of the common tidal constituents, the minimum (min) and maximum (max) difference of the particular model minus our model over a 20 years prediction interval and the RMS for each tidal constituent of the differences of the particular model minus our model are given in [nm s^{-2}]. The first two models combine the regional SEAT tide model with the global ocean tide models TPXO.7.2 and EOT08a, respectively. The following seven models were retrieved from the Ocean Tide Loading Provider based on different global tide models without explicit treatment of the Río de la Plata estuary. The last model is identical to that presented in Table 1, except the local contribution of channels and dikes according to the maximum scenario is added.

ocean tide model		SEAT +		Ocean Tide Loading Provider							incl. local channels
		TPXO.7.2	EOT08a	EOT11a	EOT08a	OSU12	TPXO.7.2	FES2012	FES2004	DTU10	
	RSS	0.66	0.70	24.79	24.97	25.69	24.98	25.13	24.95	24.63	0.005
	Min	−2.19	−1.86	−63.65	−62.84	−64.71	−62.46	−63.62	−64.38	−63.08	−0.050
	Max	2.06	2.04	79.93	80.51	83.58	81.04	81.20	79.78	78.69	0.040
	Q1	0.07	0.22	3.83	3.70	4.12	3.63	3.76	3.69	3.62	0.000
	O1	0.32	0.10	14.20	14.21	14.92	14.14	14.21	14.48	14.26	0.002
	P1	0.21	0.12	3.82	4.03	3.88	3.74	3.74	3.58	3.66	0.000
	K1	0.04	0.34	10.87	10.94	11.29	11.08	11.23	10.51	10.80	0.001
RMS	N2	0.17	0.21	4.54	4.83	5.13	5.20	5.05	4.83	4.53	0.001
	M2	0.41	0.11	15.32	15.54	15.59	15.44	15.51	15.58	15.20	0.004
	S2	0.17	0.47	3.14	2.63	2.86	2.93	2.99	3.07	2.93	0.000
	K2	0.17	0.15	0.56	0.56	0.68	0.47	0.48	0.55	0.54	0.000
	M4	0.15	0.07	–	–	–	–	–	–	–	0.000

Table 4: Comparison of alternative predictions of tidal loading effects on vertical deformation with respect to the model used in Table 2. The models and parameters are the same as for Table 3; deformation is given in [mm].

ocean tide model		SEAT +		Ocean Tide Loading Provider							incl. local channels
		TPXO.7.2	EOT08a	EOT11a	EOT08a	OSU12	TPXO.7.2	FES2012	FES2004	DTU10	
	RSS	0.14	0.14	0.69	0.62	0.46	0.32	0.35	0.71	0.82	0.001
	min	−0.41	−0.35	−2.24	−2.00	−1.62	−1.21	−1.19	−1.85	−2.37	−0.020
	max	0.37	0.38	2.20	1.97	1.89	1.03	1.17	2.37	2.30	0.020
	Q1	0.01	0.03	0.11	0.02	0.17	0.03	0.07	0.05	0.06	0.000
	O1	0.08	0.00	0.26	0.21	0.18	0.12	0.16	0.23	0.28	0.000
	P1	0.04	0.04	0.03	0.11	0.07	0.03	0.04	0.12	0.08	0.000
	K1	0.03	0.06	0.08	0.07	0.25	0.14	0.11	0.12	0.11	0.000
RMS	N2	0.00	0.02	0.25	0.15	0.08	0.06	0.06	0.18	0.27	0.000
	M2	0.07	0.03	0.55	0.50	0.25	0.24	0.26	0.60	0.70	0.001
	S2	0.03	0.10	0.15	0.21	0.05	0.04	0.04	0.14	0.06	0.000
	K2	0.06	0.02	0.02	0.05	0.12	0.06	0.07	0.06	0.09	0.000
	M4	0.05	0.02	–	–	–	–	–	–	–	0.000

tudes of the ocean tidal loading deformation reaching almost 5 mm for the M2 constituent.

The tidal (ocean and atmospheric) loading is furthermore superimposed by non-periodic loads. In particular, storm surges usually related to south-easterly winds produce sporadic events of increased water levels in the upper reaches of the estuary that may exceed 3 m [27]. This is one order of magnitude larger than the tidal water-level variations in the estuary. However, this load is confined to a narrow area compared to the ocean tides which receive their largest contribution from the open Atlantic. The 6-hourly AOD1B GRACE de-aliasing product yields non-tidal atmospheric and ocean loading deformations for the AGGO site in the range of ±1.5 cm in the period 1993-2016.

5 Conclusions and outlook

The presented tidal loading model serves the community to correct the geodetic observation data to be generated at AGGO for the effects of ocean tidal loading. The comparison of our model with conventional predictions relying purely on global ocean tide models reveals the need to incorporate a regional tide model to account for the peculiar tidal dynamics in the Río de la Plata estuary. The tidal loading at the AGGO site is dominated by the tides in the Atlantic Ocean. Local contributions from the channels, dikes and groundwater are negligible. The ocean tidal loading effects are superimposed by tidal atmospheric loading on the S1 and S2 constituents, with amplitudes slightly larger

than the ocean loading in the case of gravity and an order of magnitude smaller in the case of vertical deformation.

The determination of this model is, however, only a first step. Once observation data becomes available, especially from AGGO's superconducting gravity meter, this initial model is to be improved. Due to their superior sensitivity to loading signals, the gravity data ARE especially suited for an observational determination of the ocean tidal loading. Hence, the geometric observation techniques will also benefit from improved tidal loading corrections. In particular, gravity time series observed at AGGO will allow to expand the set of tidal constituents considered, which is at present predetermined by the global and regional tide models used in our computation. As the gravity data will accumulate continuously, it will allow us to include a growing number of additional tidal frequencies, depending on the observation record length, and thus to gradually complete the tidal spectrum.

In future, a comparison of observed tidal loading effects with our predictions will allow for a regional validation of the earth model employed in the modelling of these effects. Deviations from the rheological properties implied by the globally uniform Gutenberg-Bullen earth model have been reported from other regions [28]. Such a validation is thus of particular interest given the peculiarities of the geological and hydrogeological setting of the AGGO site. On the other hand, recent research has suggested non-elastic contributions to tidal loading effects [29]. This calls for further investigation towards its incorporation in the general computation procedure of loading effects and the applied earth models.

However, the significance of the conclusions of this validation will depend directly on the precision of the load model introduced in the prediction of tidal loading effects. In this context, we recommend the installation and operation of a new tide gauge in the immediate vicinity of AGGO.

References

[1] Wziontek H., Nowak I., Hase H., Häfner M., Güntner A., Reich M. et al., 2016, A new gravimetric reference station in South America: The installation of the superconducting gravimeters SG038 at the Argentine-German Geodetic Observatory AGGO, Geophys. Res. Abstracts, 18, EGU2016-12612.

[2] Petit G and Luzum B., 2010, IERS Conventions (2010), Technical Report 36, IERS Conventions Centre.

[3] Guerrero R.A., Acha E.M., Framiñan M.B. and Lasta C.A., 1997, Physical oceanography of the Río de la Plata estuary, Argentina, Cont. Shelf Res., 17, 727-742.

[4] Simionato C.G., Dragani W., Meccia V. and Nuñez M., 2004, A numerical study of the barotropic circulation of the Río de la Plata estuary: sensitivity to bathymetry, the Earth's rotation and low-frequency wind variability, Estuar. Coast. Shelf S., 61, 261-273.

[5] Simionato C.G., Dragani W., Nuñez M. and Engel M., 2004b, A set of 3-D nested models for tidal propagation from the Argentine continental shelf tot he Río de la Plata estuary – Part 1. M2, J. Coastal Res., 20, 3, 893-912.

[6] Stammer D., Ray R.D., Andersen O.B., Arbic B.K., Bosch W., Carrère L. et al., 2014, Accuracy assessment of global barotropic ocean tide models, Rev. Geophys., 52, 3, 243-282, doi:10.1002/2014RG000450.

[7] Andersen O.B. and Scharoo R., 2011, Range and geophysical corrections in coastal regions and implicationsfor mean sea surface determination. In: S. Vignudelli, A. Kostianoy, P. Cipollini, J. Benveniste (Eds.), Coastal Altimetry, Springer, Berlin, ISBN: 978-3-642-12795-3.

[8] D'Onofrio E., Oreiro F., and Fiore M., 2012, Simplified Empirical Astronomical Tide model - an application for the Río de la Plata estuary, Comput. Geosci., 44, 196-202.

[9] Klügel T. and Wziontek H., 2009, Correcting gravimetrs and tiltmeters for atmospheric mass attraction using operational weather models, J. Geodyn., 48, 3-5, 204-210, doi:10.1016/j.jog.2009.09.010.

[10] Bos M.S. and Scherneck H.-G., http://holt.oso.chalmers.se/loading#select

[11] Pagiatakis S., 2007, The response of a realistic Earth to ocean tide loading, Geophys. J. Int., 103, 2), 541-560, doi:10.1111/j.1365-246X.1990.tb01790.x

[12] Farrell W.E., 1972, Deformation of the Earth by Surface Loads, Rev. Geophys. Space Phys., 10, 3, 761-797.

[13] Blewitt G., 2003, Self-consistency in reference frames, geocenter definition, and surface loading of the solid Earth, J. Geophys. Res., 108, B2, doi:10.1029/2002JB002082.

[14] Agnew D.C., 1997, NLOADF: A program for computing ocean-tide loading, J. Geophys. Res., 102, B3, 5109-5110.

[15] Savcenko R. and Bosch W., 2012, EOT11a − Empirical ocean tide model from multi-mission satellite altimetry, DGFI Report 89, Deutsches Geodätisches Forschungsinstitut, München, Germany.

[16] Savcenko R. and Bosch W., 2008, EOT08a − Empirical ocean tide model from multi-mission satellite altimetry, DGFI Report 81, Deutsches Geodätisches Forschungsinstitut, München, Germany.

[17] Egbert G.D. and Erofeeva L, 2002, Efficient inverse modelling of barotropic ocean tides, J. Atmos. Ocean. Tech., 19.

[18] Wenzel H., 1996, The nanogal software: Earth tide processing package ETERNA 3.30, Bull. Inf. Mar. Terr., 124, 9425-9439.

[19] Ray R.D. and Ponte R.M., 2003, Barometric tides from ECMWF operational analyses. Ann. Geophys., 21, 8, 1897-1910, doi:10.5194/angeo-21-1897-2003.

[20] Fritsche M., Sosnica K., Rodriguez-Solano C.J., Steigenberger P., Wang K. K., Dietrich R. et al., 2014, Homogeneous reprocessing of GPS, GLONASS and SLR observations. J. Geodesy, 88, 7, 625-642, doi:10.1007/s00190-014-0710-3.

[21] Fok H.S., Shum C.K., Yi Y., Iz H.B. and Matsumoto K., 2012, Improved coastal ocean tide modelling using satellite altimetry, In: Proceedings of Meeting 20 Years of Progress in Radar Altimetry (24-29 September 2012, Venice-Lido, Italy), Venice.

[22] Carrère L., Lyard F., Cancet M., Guillot A. and Roblou L., 2012, A new global tidal model taking advantage of nearly 20 years of altimetry. In: Proceedings of Meeting 20 Years of Progress in Radar Altimetry (24-29 September 2012, Venice-Lido, Italy), Venice.

[23] Lyard L., Lefevre L., Letellier T. and Francis O., 2006, Modelling the global ocean tides: insights from FES2004, Ocean Dynam., 56, 394-415.

[24] Cheng Y. and Andersen O.B., 2010, Improvement in global ocean tide model in shallow water regions. OSTST Meeting, SV.1-68 45, Lisbon.

[25] Saraceno M., D'Onofrio E.E., Fiore M.E. and Grismeyer W.H., 2010, Tide model comparison over the Southwestern Atlantic Shelf, Cont. Shelf Res., 30, 1865-1875, doi:10.1016/j.csr.2010.08.014.

[26] Murray M.T., 1964, A general method for the analysis of hourly heights of the tide, Int. Hydrogr. Rev., 41, 2, 91-101.

[27] D'Onofrio E., Fiore M.M.E. and Romero S., 1999, Return periods of extreme water levels estimated for some vulnerable areas of Buenos Aires, Cont. Shelf Res., 19, 1681-1693.

[28] Richter A., Hormaechea J.L., Dietrich R., Perdomo R. R., Fritsche M., Del Cogliano D. et al., 2009, Anomalous oean load tide signal observed in lake-level variations in Tierra del Fuego. Geophys. Res. Lett., 36, L05305, doi:10.1029/2008GL036970.

[29] Bos M.S., Penna N., Baker T.F. and Clarke P.J., 2015, Ocean tide loading displacements in western Europe. Part 2: GPS-observed anelastic dispersion in the asthenosphere, J. Geophys. Res., 120, 9, doi:10.1002/2015JB011884.